Calcium-dependent block of P2X7 receptor channel function is allosteric

Zonghe Yan,[1] Anmar Khadra,[2] Arthur Sherman,[2] and Stanko S. Stojilkovic[1]

[1]Section on Cellular Signaling, Program in Developmental Neuroscience, National Institute of Child Health and Human Development and [2]Laboratory of Biological Modeling, National Institute of Diabetes and Digestive and Kidney Diseases, National Institutes of Health, Bethesda, MD 20892

Among purinergic P2X receptor (P2XR) channels, the P2X7R exhibits the most complex gating kinetics; the binding of orthosteric agonists at the ectodomain induces a conformational change in the receptor complex that favors a gating transition from closed to open and dilated states. Bath Ca^{2+} affects P2X7R gating through a still uncharacterized mechanism: it could act by reducing the adenosine triphosphate^{4-} (ATP^{4-}) concentration (a form proposed to be the P2X7R orthosteric agonist), as an allosteric modulator, and/or by directly altering the selectivity of pore to cations. In this study, we combined biophysical and mathematical approaches to clarify the role of calcium in P2X7R gating. In naive receptors, bath calcium affected the activation permeability dynamics indirectly by decreasing the potency of orthosteric agonists in a concentration-dependent manner and independently of the concentrations of the free acid form of agonists and status of pannexin-1 (Panx1) channels. Bath calcium also facilitated the rates of receptor deactivation in a concentration-dependent manner but did not affect a progressive delay in receptor deactivation caused by repetitive agonist application. The effects of calcium on the kinetics of receptor deactivation were rapid and reversible. A438079, a potent orthosteric competitive antagonist, protected the rebinding effect of 2'(3')-*O*-4-benzoylbenzoyl)ATP on the kinetics of current decay during the washout period, but in the presence of A438079, calcium also increased the rate of receptor deactivation. The corresponding kinetic (Markov state) model indicated that the decrease in binding affinity leads to a decrease in current amplitudes and facilitation of receptor deactivation, both in an extracellular calcium concentration–dependent manner expressed as a Hill function. The results indicate that calcium in physiological concentrations acts as a negative allosteric modulator of P2X7R by decreasing the affinity of receptors for orthosteric ligand agonists, but not antagonists, and not by affecting the permeability dynamics directly or indirectly through Panx1 channels. We expect these results to generalize to other P2XRs.

INTRODUCTION

Purinergic P2X receptors (P2XRs) are ATP-gated cation channels. Seven mammalian receptor subunits, denoted P2X1 through P2X7, and several spliced forms of these subunits have been identified. Each subunit has only two transmembrane (TM) domains, the N and C termini facing the cytoplasm, and a large extracellular loop. These subunits assemble together as homo- or heterotrimers to make functional receptors (North, 2002). P2XRs likely have three intersubunit orthosteric binding sites located in the ectodomain, and their full occupancy appears to be required for conformational changes in the TM channel gate, leading to facilitation of cation influx through the channel pore (Marquez-Klaka et al., 2007; Browne et al., 2010). All P2XRs are permeable to Na^+, K^+, and Ca^{2+}, and some are also permeable to Cl^- (Egan et al., 2006). Positive and negative allosteric modulators of P2XRs interact with binding sites that are topologically distinct from the orthosteric sites recognized by the receptor endogenous agonist ATP, causing conformational changes that profoundly influence the gating of P2XRs (Coddou et al., 2011). In general, it is difficult to explore experimentally the interactions between binding of orthosteric and allosteric ligands and gating because simultaneous assessment of ligand binding and channel gating is not possible. Therefore, understanding ligand-gated systems predominantly depends on development of a kinetic model (Colquhoun, 1998).

The P2X7R is an unusual member of this family of channels. Structurally, the P2X7 subunit is distinguished from other subunits by its long intracellular C-terminal tail containing multiple protein and lipid interaction motifs and a cysteine-rich 18–amino acid segment (Surprenant et al., 1996) and by its inability to make stable heteromeric complexes (Torres et al., 1999; Nicke, 2008). It also appears that this channel exhibits different permeability states (Yan et al., 2008), which

Correspondence to Stanko S. Stojilkovic: stankos@helix.nih.gov

Abbreviations used in this paper: BzATP, 2'(3')-*O*-4-benzoylbenzoyl)ATP; CBX, carbenoxolone; HEK, human embryonic kidney; TM, transmembrane.

The Rockefeller University Press $30.00
J. Gen. Physiol. Vol. 138 No. 4 437–452
www.jgp.org/cgi/doi/10.1085/jgp.201110647

further complicates the understanding of coupling of conformational changes in the orthosteric binding domains with the corresponding changes at the TM channel gate. The binding of Ca^{2+} and Mg^{2+} to β- and γ-phosphate groups of ATP is a well-established phenomenon (Jahngen and Rossomando, 1983), but at the present time it is unknown which form of ATP (ATP^{4-} and/or Mg/Ca-ATP) acts as an orthosteric agonist for this receptor (Jiang, 2009). It has also not been clarified whether these two macroelements affect the receptor function by acting as allosteric modulators, as earlier data suggest (Virginio et al., 1997), and/or by altering the permeability dynamics, as shown for P2X4R (Khakh et al., 1999). Furthermore, it is unknown how allosteric modulators affect P2X7R gating by changing the affinity of receptors for ATP and/or the strength of gating, i.e., the transduction of signals from orthosteric binding domains to the receptor gate. Finally, the interaction between allosteric agonists/antagonists and orthosteric antagonists has not been examined previously for P2X7R.

In this study, we combined biophysical and mathematical approaches to address these questions. To examine the influence of bath Ca^{2+} on the permeability dynamics, we performed full concentration response studies using ATP and 2'(3')-*O*-4-benzoylbenzoyl)ATP (BzATP) as orthosteric agonists in naive cells (not previously exposed to orthosteric agonists) bathed in Ca^{2+}-containing and Ca^{2+}-deficient medium. To clarify whether Ca^{2+} affects P2X7R by reducing the free acid concentration of agonist, we manipulated total agonist and Ca^{2+} concentration, resulting in either fixed or progressively increased free acid agonist concentration. We also studied the influence of Ca^{2+} on receptor behavior by analyzing the rates of decay of current after washout of agonists or application of a competitive orthosteric antagonist, termed current or receptor deactivation. Based on experimental data, we revised a previously published Markov state model (Yan et al., 2010) to describe regulation of P2X7R by bath calcium, which provides a better understanding of the dynamics of these receptors under orthosteric and allosteric regulation.

MATERIALS AND METHODS

Cell culture and transfection

Human embryonic kidney 293 (HEK293) cells were used for the expression of wild-type and mutant P2X7Rs, as described previously (He et al., 2003; Yan et al., 2006). These cells were obtained from the American Type Culture Collection and were routinely maintained in Dulbecco's modified Eagle's medium containing 10% (vol/vol) fetal bovine serum (Invitrogen) and 1% (vol/vol) penicillin–streptomycin liquid (Invitrogen) in a tissue culture incubator. For electrophysiological measurements, cells were grown on 35-mm dishes at a density of 0.5×10^6 cells per dish. Transfection was conducted 24 h after plating the cells using 2 µg DNA and 5 µl Lipofectamine 2000 reagent (Invitrogen) in 2 ml of serum-free Opti-MEM (Invitrogen). After 4.5 h of incubation, the transfection mixture was replaced with normal culture medium, and cells were cultured for an additional 24–48 h. Transfected cells were mechanically dispersed and recultured on 35-mm dishes for 2–10 h.

Current measurements

Whole-cell patch-clamp recordings were performed with single cells at room temperature using an Axopatch 200B amplifier (Axon Instruments) as described previously (Yan et al., 2005). Patch electrodes, fabricated from borosilicate glass (type 1B150F-3; World Precision Instruments, Inc.) using a Flaming Brown horizontal puller (P-97; Sutter Instrument), were heat polished to a final tip resistance of 3.5–5.5 Mohm. All current recordings were programmed, captured, and stored using the pClamp 8.0 software packages in conjunction with a converter (Digidata 1322A A/D; Axon Instruments). Experiments were performed on single cells with a mean capacitance of 10 pF. Unless otherwise stated, membrane potential was held at −60 mV. Current–voltage relations were used to estimate changes in reversal potential during agonist application and were obtained by voltage ramps from −80 to 80 mV delivered twice per second during 50 s. Patch electrodes were filled with solution containing 145 mM NaCl, 10 mM EGTA, and 10 mM HEPES; the pH was adjusted with 10 M NaOH to 7.35. The osmolarity of this solution was 305 mosM. Krebs-Ringer–like bath buffer contained 147 mM NaCl, 3 mM KCl, 1 mM $MgCl_2$, 0–10 mM $CaCl_2$, 10 mM glucose, and 10 mM HEPES; the pH was adjusted to 7.35 with 10 M NaOH. In some experiments, ATP and BzATP solutions were prepared daily in bath buffer with pH properly readjusted and were applied using either an Ultrafast Solution-Switching System (LSS-3200; EXFO Burleigh Products Group Inc.) that was simultaneously program controlled by pClamp 8.0 software through a PZ-150M amplifier (Yan et al., 2006) or an RSC-200 Rapid Solution Changer (Biological). Cells with enhanced green fluorescent protein fluorescence were identified before immersing the electrode in bath solution for a gigaohm seal.

Measurements of free calcium concentrations in bath medium

Measurements of free calcium ion concentration in bath medium with or without ATP and BzATP were made with a plastic membrane combination calcium ion selective electrode (ionplus Sure-Flow; Thermo Fisher Scientific). ATP (Sigma-Aldrich) and BzATP (Sigma-Aldrich) were weighed to prepare the 10-mM stock solution in deionized water according to the free acid formula weight on the product label. The Mg^{2+}-free sodium background buffer consisted of 147 mM NaCl, 3 mM KCl, 10 mM glucose, and 10 mM HEPES, and the pH was properly adjusted to 7.35 with NaOH. The 0.95-mM Ca^{2+} buffer was prepared by addition of 0.1 M Ca^{2+} standard (Thermo Fisher Scientific) to the background buffer. 320-, 100-, 32-, 10-, 3.2-, 1-, and 0-µM ATP or BzATP solutions were prepared by addition of the same 480-µl sum volume of various combinations of pure water and 10-mM ATP or BzATP stock solution into the 19.6 ml of 0.95-mM Ca^{2+} buffer. To generate a standard curve, a real-time recording of the millivolt reading of the calcium ion selective electrode was performed with an Orion 4-Star reader (Thermo Fisher Scientific), and the standard curve was calculated by semilogarithmic fitting using KaleidaGraph v 4.1 (Synergy Software). After the standard curve recording, the millivolt readings of different ATP or BzATP solutions were collected, and the test-free Ca^{2+} concentrations were derived from the standard curve.

Calculations

Whenever appropriate, the data were presented as mean ± SEM values. Significant differences, with $P < 0.01$, were determined by Mann-Whitney test using InStat 3.05 (GraphPad Software). Nonlinear curve fitting of deactivation currents was performed with the

Clampfit 10.0 (Molecular Devices) predefined biexponential function ($f(t) = A_1 \exp(-t/\tau_1) + A_2 \exp(-t/\tau_2)$). ATP^{4-} and $BzATP^{4-}$ concentrations were calculated using Theo Schoenmakers' program Chelator, which is freely available online. Numerical simulations of the Markov state model were performed using MATLAB (Mathworks). Parameter fitting of f to the simulations of the Markov state model over the interval $[a,b]$ was performed by minimizing the error given by the L_2 norm

$$\left\| f - \tilde{f} \right\| = \left\{ \frac{1}{b-a} \int_a^b \left[f(t) - \tilde{f}(t) \right]^2 dt \right\}^{0.5}.$$

Kinetic model

A Markov state model consisting of eight states (C_i, closed states and Q_i, open states, i = 1–4) describing the sequence of binding and unbinding of agonist to P2X7R was used (Fig. S2). Details of the scheme are available in Yan et al. (2010). In brief, each state corresponds to the fraction of receptors that are either unsensitized or sensitized (Fig. S2, top and bottom row, respectively) with a given number of agonist binding sites occupied. Negative cooperativity in agonist binding (i.e., a decrease in binding affinity with the occupation of each site) is assumed to occur only to unsensitized receptors (Fig. S2, top row). However, receptor sensitization (Fig. S2, bottom row) is assumed to restore symmetry of agonist binding and lead to dilation of the channel associated with each receptor. The allosteric binding of divalent extracellular Ca^{2+} to the P2X7R has been added to the model as a new feature. This is done by assuming that the forward rates (k_2, k_4, and k_6) decrease by a factor F and the backward rates (k_1, k_3, and k_5) increase by a factor $(2 - F)$ when bath extracellular calcium concentration ($[Ca^{2+}]_e$) is increased. When $F = 1$, the model reduces to the previously published version, and this happens when $[Ca^{2+}]_e \approx 2$ mM. F is a decreasing Hill function (Fig. S3) and is given by

$$F = \alpha \frac{\beta^2}{\beta^2 + [DC]_e^2},$$

where α is the maximum level of allosteric regulation (or inhibition) and β is the half-maximum level of divalent cations ($[DC]_e$) required for such regulation.

The mathematical model associated with this Markov state model (shown schematically in Fig. S2) is thus given by

$$\frac{dC_1}{dt} = k_1(2-F)C_2 + L_1C_4 - 3k_2AFC_1, \quad (1)$$

$$\frac{dC_2}{dt} = 3k_2AFC_1 + 2k_1(2-F)Q_1 - (2k_4AF + k_1(2-F))C_2, \quad (2)$$

$$\frac{dQ_1}{dt} = 2k_4AFC_2 + 3k_5(2-F)Q_2 - (2k_3(2-F) + k_6AF)Q_1, \quad (3)$$

$$\frac{dQ_2}{dt} = k_6AFQ_1 + L_2Q_3 - (3k_5(2-F) + L_3)Q_2, \quad (4)$$

$$\frac{dQ_3}{dt} = k_2AFQ_4 + L_3Q_2 - (3k_1(2-F) + L_2)Q_3, \quad (5)$$

$$\frac{dQ_4}{dt} = 2k_2AFC_3 + 3k_1(2-F)Q_3 - (2k_1(2-F) + k_2AF)Q_4, \quad (6)$$

$$\frac{dC_3}{dt} = 3k_2AFC_4 + 2k_1(2-F)Q_4 - (k_1(2-F) + 2k_2AF)C_3, \quad (7)$$

$$\text{and } \frac{dC_4}{dt} = k_1(2-F)C_3 - (L_1 + 3k_2AF)C_4, \quad (8)$$

where A is the applied agonist concentration and L_i, i = 1–3, are the rates of sensitization/loss of sensitization. The whole-cell current is then given by

$$I = g_{12}(Q_1 + Q_2)(V - E) + g_{34}(Q_3 + Q_4)(V - E), \quad (9)$$

where g_{12} is the conductance of the Q_1 and Q_2 states and g_{34} is the conductance of the Q_3 and Q_4 states ($g_{12} < g_{34}$), V is the holding potential, and E is the reversal potential (see Table S1 for parameter values). Although it is possible to model the allosteric binding of Ca^{2+} to P2X7R by adding new states to the scheme, each representing the fraction of receptors with a given number of occupied allosteric Ca^{2+} binding sites (as well as occupied orthosteric agonist binding sites), the total number of these allosteric binding sites is not known, and the complexity of the scheme would become unnecessarily large. For this reason, we model the effects of divalent cations using the aforementioned phenomenological approach.

Online supplemental material

Fig. S1 shows the effects of a P2X7R-specific antagonist on BzATP-induced receptor activation and deactivation. Fig. S2 shows a Markov state model describing the binding and unbinding of BzATP to the P2X7R. Fig. S3 illustrates Hill functions describing allosteric regulation of P2X7R by divalent cations, whereas Fig. S4 illustrates the effects of divalent cations on receptor deactivation. Table S1 shows parameter values and distributions used in modeling of P2X7R gating. Online supplemental material is available at http://www.jgp.org/cgi/content/full/jgp.201110647/DC1.

RESULTS

Extracellular calcium dependence of orthosteric agonist potency

To clarify whether bath Ca^{2+} plays a role in the P2X7R permeability kinetics, we studied the concentration dependence of ATP and BzATP on currents using the wild-type rat P2X7R expressed in HEK293 cells bathed in 2-mM Ca^{2+}/1-mM Mg^{2+}–containing buffer or in Ca^{2+}-deficient/1-mM Mg^{2+}–containing buffer. All experiments were performed with naive receptors (not previously exposed to agonist), and all recordings were performed in one cell per dish during a single agonist application/withdrawal. Fig. 1 illustrates the patterns of current responses in cells stimulated with ATP (A and B) and BzATP (C and D) for 40 s or 2 min in 2-mM Ca^{2+}–containing (A and C) and Ca^{2+}-deficient (B and D) medium. In cells bathed in Ca^{2+}–containing medium, monophasic, slowly developing currents of small amplitude were observed in response to 0.1 and 0.32 mM ATP (Fig. 1 A) and 3.2 and 10 µM BzATP (Fig. 1 C). As described previously (Yan et al., 2008, 2010), at higher agonist concentrations (1–10 mM ATP and 32–320 µM BzATP), biphasic currents were observed, with a rapid initial rise in current (I_1) followed by a slower secondary rise (I_2) that we interpret as dilation of the pore.

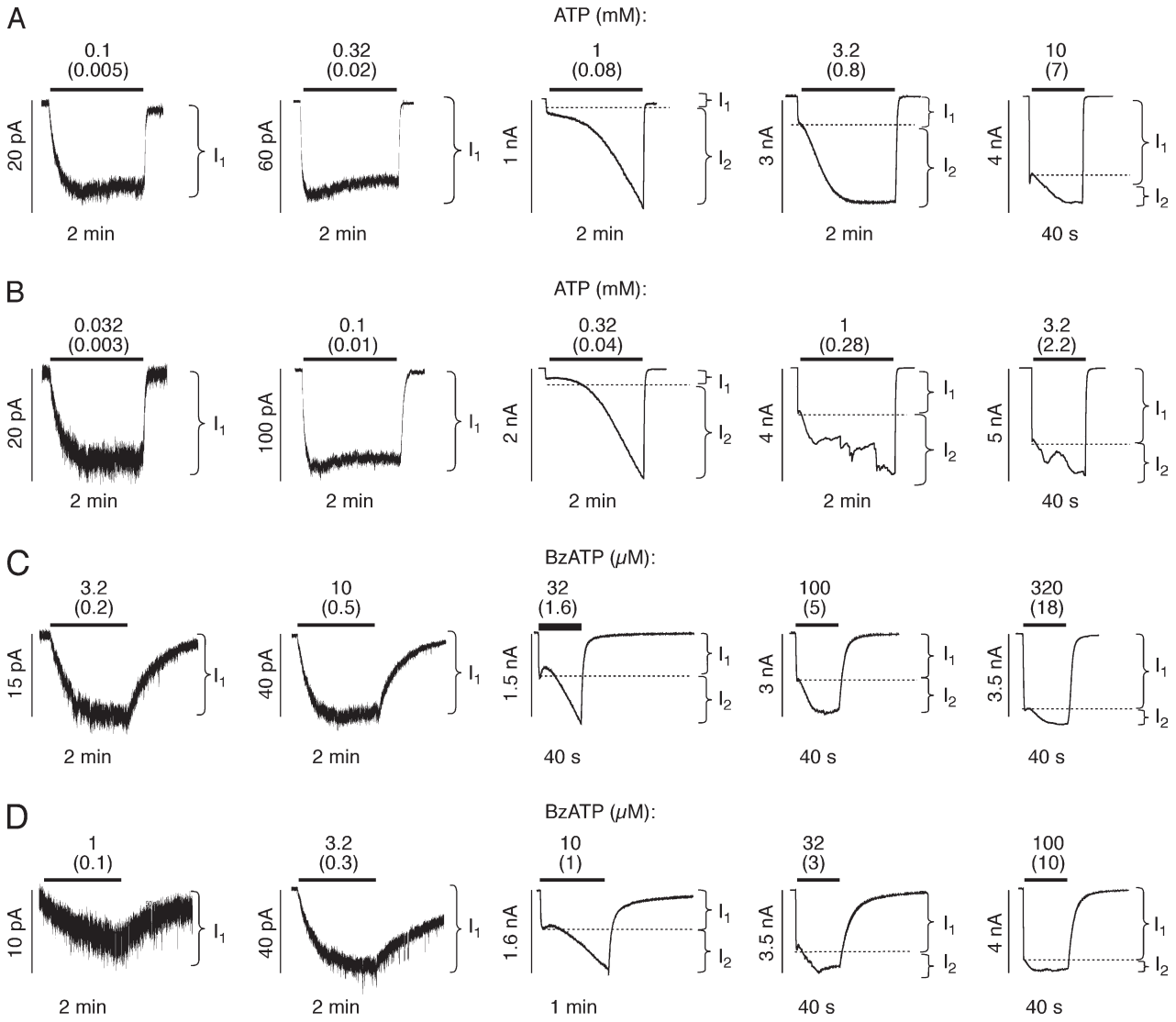

Figure 1. Effects of bath calcium on P2X7R current. (A–D) Concentration dependence on ATP (A and B) and BzATP (C and D) of P2X7R current in single HEK293 cells bathed in 2-mM Ca^{2+}–containing (A and C) and Ca^{2+}-deficient (B and D) medium with 1 mM Mg^{2+}. In this and following figures, the whole-cell current recording was performed using Ca^{2+}-deficient pipette medium containing 10 mM EGTA, and cells were held at −60 mV, if not otherwise specified. Horizontal bars above traces indicate the duration of agonist application. The current response was monophasic at low agonist concentrations and biphasic at higher concentrations. The ratio between rapid (I_1) and sustained (I_2) currents also changed with the increase in agonist concentration, as described previously (Yan et al., 2010). All traces shown were obtained during the initial agonist application and are representative of at least five records per dose. Mean ± SEM values are shown in Fig. 2 A. Numbers without parentheses indicate total agonist concentrations used in experiments, and numbers in parentheses indicate free agonist concentration calculated using the Maxc program for two chelators and two metals. The responses to ATP (A vs. B) and BzATP (C vs. D) were similar when the free concentration of each agonist was similar. However, there was a Ca^{2+}-dependent shift in the dose–response of ∼0.5 log units of total agonist concentration. Dotted lines separate I_1 and I_2 currents.

The rate of dilation increased with elevation in agonist concentrations until, at the highest agonist concentrations, the channels passed almost immediately to the dilated state, and the current consisted mostly of I_1, as it did for the lowest agonist concentrations. The same pattern of response was also observed in cells bathed in Ca^{2+}-deficient medium, but with a leftward shift in agonist concentration of ∼0.5 log units (Fig. 1, B and D; and Fig. 2 A). The "noise" current observed in response to 1 and 3.2 mM ATP does not reflect low quality recording but temporally coincides with extensive blebbing. Others have observed similar effects (Roger et al., 2008). Because the development of biphasic current reflects a transition from an open to a dilated state, these results indicate that the pore does not depend on bath Ca^{2+}.

The calculated values of ATP^{4-} concentrations in Ca^{2+}-containing and -deficient media are shown in Fig. 1 (A and B; numbers in parentheses above traces). Using the same program (the Maxc program for a two-chelator, two-metal calculation), we also calculated the concentration

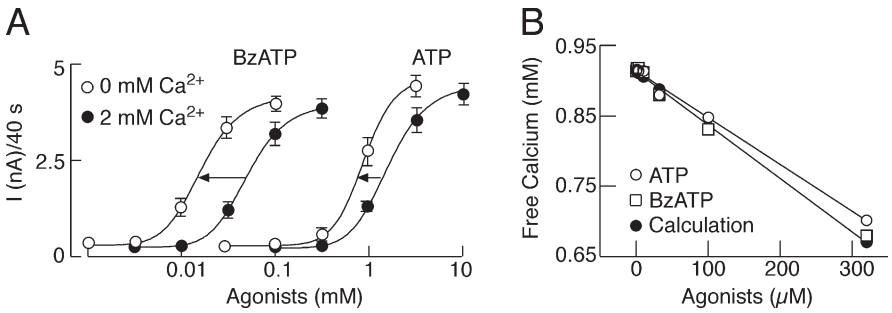

Figure 2. The relationship between bath calcium and P2X7R agonists. (A) Concentration-dependent effects of ATP and BzATP on the peak amplitude of current in cells bathed in Ca^{2+}-deficient (open circles) and 2-mM Ca^{2+}–containing (closed circles) medium. The amplitude of current was measured after 40 s of agonist application. Data shown are mean ± SEM values from at least four responses per dose during initial agonist applications. Representative traces are shown in Fig. 1. Arrows indicate leftward shifts in EC_{50} values, reflecting an increase in sensitivity to agonist stimulation in Ca^{2+}-deficient medium. (B) Concentration-dependent effects of ATP and BzATP on free Ca^{2+} concentration. The background buffer contained 147 mM NaCl, 3 mM KCl, 10 mM glucose, and 10 mM HEPES supplemented with 0.95 mM Ca^{2+}. Free Ca^{2+} concentration was measured with a calcium ion selective electrode as described in Materials and methods. Data shown are means from three experiments, and SEM values are within the symbols. The calculated free calcium concentrations were obtained using the Maxc program.

of the free acid form of BzATP in solution (Fig. 1, C and D). Comparing the values of the calculated free acid forms of the two agonists in Ca^{2+}-containing and Ca^{2+}-deficient medium indicates practically identical concentration responses in the absence and presence of Ca^{2+}. This is consistent with a hypothesis that ATP^{4-} rather than the divalent-bound ATP is the native agonist for this receptor subtype. However, these results are also consistent with the hypothesis that bath Ca^{2+} acts as an allosteric inhibitor and that 2 mM Ca^{2+} causes a rightward shift in the potency of agonists of ~0.5 log units independent of the concentration of the free acid form of agonists. In the next section, we consider experiments to distinguish between the two hypotheses.

Concentration dependence of agonist potency on extracellular calcium

In further experiments, we varied bath Ca^{2+} concentrations (0.5, 1, 2, 5, and 10 mM), keeping identical (100 μM) total BzATP concentrations and 1 mM Mg^{2+} in buffer solution. Fig. 3 A shows that the calculated free acid concentrations of BzATP progressively decreased with an increase in bath Ca^{2+} concentration. Representative traces of current responses during the initial agonist application are shown in Fig. 3 B. Application of media containing 100 μM BzATP and 0.5 mM Ca^{2+} resulted in high amplitude biphasic currents, whereas the current amplitude decreased with an increase in bath Ca^{2+} concentrations to 5 and 10 mM. Fig. 3 C shows the correlation between divalent cation concentrations and amplitude of current response (left) and between free BzATP concentration and amplitude of current response (right) using mean ± SEM values. A similar correlation coefficient was observed in both cases, indicating that these experiments could not distinguish between the two hypotheses for the action of bath Ca^{2+} as either an allosteric modulator (Fig. 3 C, left) or a factor determining free agonist concentration (Fig. 3 C, right).

One way to overcome this limitation is to have variable Ca^{2+} concentrations and identical free agonist concentrations. As estimated by the Maxc program calculations, these types of experiments are practically impossible to do with ATP because it acts as an orthosteric agonist for P2X7R in the submillimolar to millimolar concentration range. Specifically, binding of divalent cations to ATP in this concentration range affects not only the free agonist concentration but also the free divalent cation concentrations. Thus, to have minimum impact on divalent cation concentrations, an agonist should be at least in a micromolar concentration range, which is the case with BzATP. As shown in Fig. 3 D, calculations indicated that the free acid form of BzATP could be fixed at 1.6 μM by varying the total BzATP concentration from 17 to 90 μM and the total Ca^{2+} concentration from 0 to 10 mM in the presence of constant (1 mM) Mg^{2+}.

However, this analysis is based on the assumption that BzATP binds calcium with a similar potency as ATP. Others have also estimated free BzATP concentration using an ATP binding program (Virginio et al., 1997). To test the validity of the calculation method for free BzATP concentration, we used a calcium ion selective electrode to estimate free bath Ca^{2+} concentrations in the presence of variable concentrations of ATP and BzATP. To exclude the impact of Mg^{2+} on calcium measurements, we used Mg^{2+}-free buffer with Ca^{2+} fixed at 950 μM and with ATP and BzATP concentrations of 0, 1, 3.2, 10, 32, 100, and 320 μM. Fig. 2 B shows highly comparable concentration-dependent effects of ATP on free Ca^{2+} concentration obtained by calculations and by measurements, confirming the validity of this method. At 0–100-μM concentration, there was no significant difference between values of free Ca^{2+} in the presence of ATP and BzATP, whereas at higher agonist concentrations, free Ca^{2+} concentrations were 2–3% higher in the presence of BzATP than ATP. These results indicate that BzATP at the concentrations used in

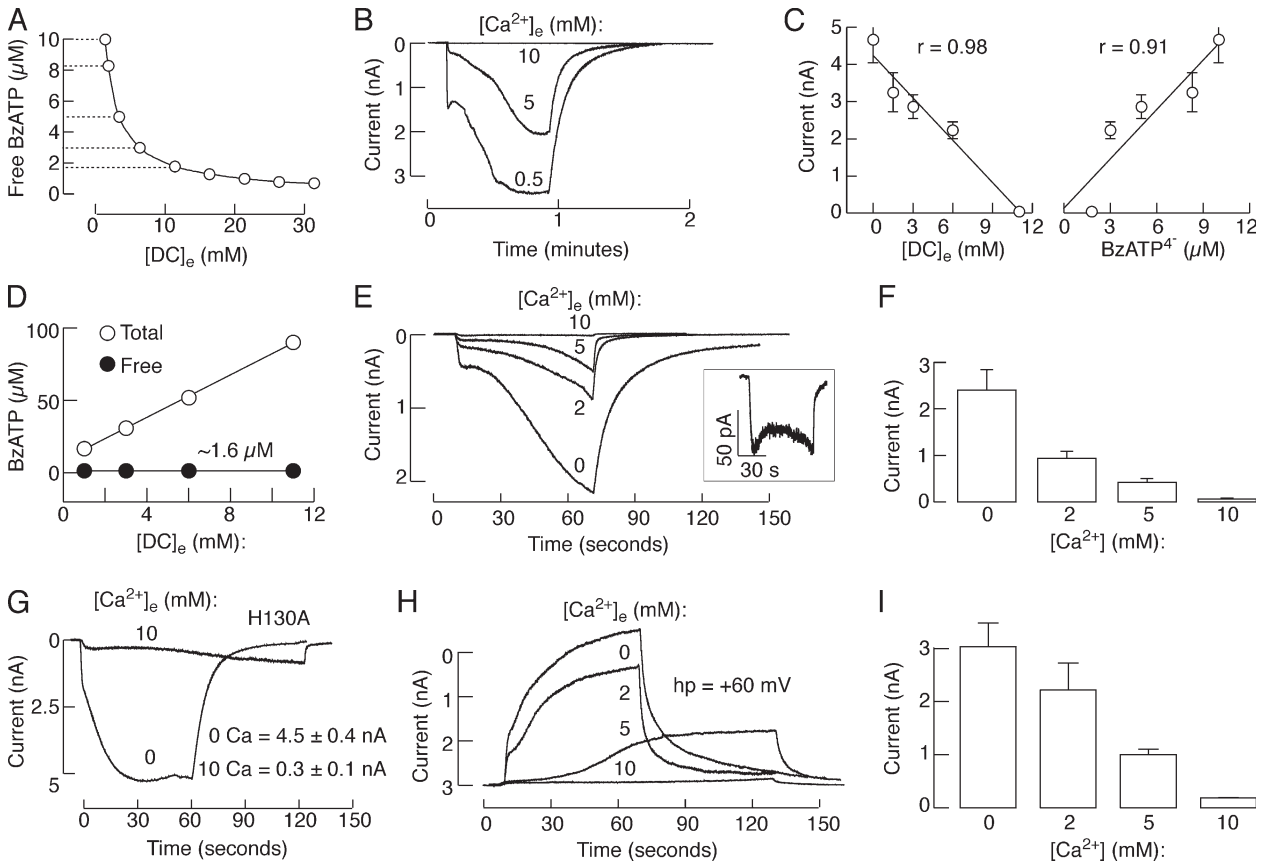

Figure 3. Dependence on extracellular Ca^{2+} concentration of BzATP-induced P2X7R current. (A) Calculated free BzATP concentration in medium containing 100 μM BzATP and variable concentrations of Ca^{2+} in the presence of 1 mM Mg^{2+}. Horizontal dotted lines indicate solutions used for activation of P2X7R shown in B and C. (B) Typical patterns of P2X7R current in response to application of 100 μM BzATP in medium containing 0.5, 5, and 10 mM Ca^{2+}. (C) Correlation between divalent cation concentrations ($[DC]_e$) and peak amplitude of current responses (left) and between free BzATP concentration and peak amplitude of current response (right). r, correlation coefficient. Data shown are means ± SEM ($n = 4$ per data point). (D–F) Variable current responses in cells stimulated with media containing identical free BzATP but variable Ca^{2+} concentrations. (D) Comparable free BzATP concentrations achieved with variable total BzATP, 1 mM Mg^{2+}, and variable Ca^{2+} concentrations. (E) A decrease in the amplitude of currents in response to media containing identical free BzATP concentrations (1.6 μM) but increasing Ca^{2+} concentrations. Inset shows the current response to medium containing 10 mM Ca^{2+} on an enlarged scale. (F) Mean ± SEM values of peak current amplitude measured 40 s after application of BzATP. $n = 4$–6 per data point. (G) Effects of bath Ca^{2+} on the peak amplitude of current in cells expressing the P2X7R-H130A mutant; representative traces and mean ± SEM values from four experiments. (H and I) Concentration-dependent effects of bath Ca^{2+} on the activation time and peak amplitude of current; representative traces (H) and mean ± SEM values from four experiments (I). hp, holding potential.

our experiments binds Ca^{2+} with a comparable capacity to ATP.

Fig. 3 (E and F) summarizes the results of stimulation of cells with BzATP and bath Ca^{2+} in concentrations shown in Fig. 3 D. Under such experimental conditions, the relationship between total agonist concentration and the pattern of current response was lost. Practically, the lowest total BzATP concentration (17 μM) was most effective, and the highest concentration (90 μM) was the least effective. Furthermore, although the free acid from of BzATP was identical in all four media, we still observed the full concentration-dependent inhibitory effect of Ca^{2+} on the peak amplitude of current response. The finding that bath Ca^{2+} affects P2X7R gating independently of the concentrations of the free acid form of agonists indicates the allosteric nature of action of this cation.

Others have shown that the rP2X7R-H130A mutant is resistant to Mg^{2+} inhibition (Acuña-Castillo et al., 2007). To examine whether this residue also accounts for allosteric action of Ca^{2+}, we stimulated cells with 100 μM BzATP in Ca^{2+}-deficient and 10-mM Ca^{2+}–containing medium. Like the wild-type receptor, the mutant receptor also responded to agonist application with a delay in receptor activation and 15-fold decrease in the peak amplitude of current when bathed in 10 mM Ca^{2+} (Fig. 3, B and G). This indicates that different residues account for the allosteric action of Ca^{2+} and Mg^{2+}.

Cells expressing wild-type receptors and clamped at 60 mV also responded to agonist application with biphasic currents, but the current was outward (Fig. 3 H). Furthermore, Ca^{2+} inhibited receptor activation in a

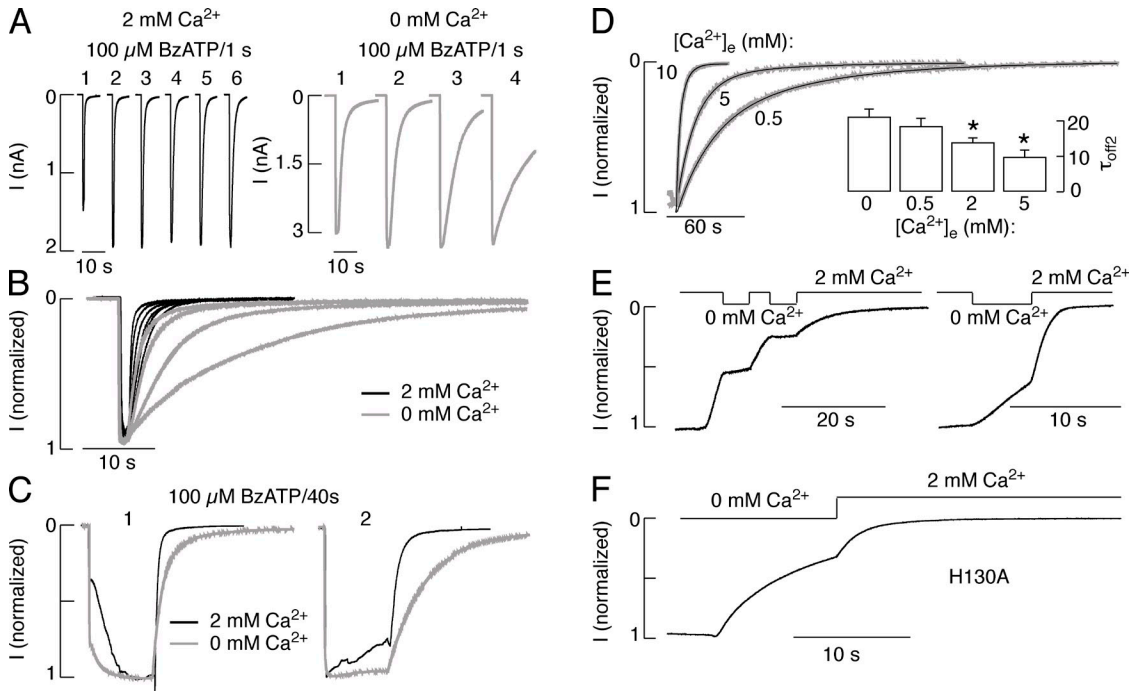

Figure 4. Calcium dependence of P2X7R deactivation. (A) Repetitive 1-s application of BzATP in cells bathed in 2 mM Ca^{2+} + 1 mM Mg^{2+} (six applications, left) and Ca^{2+}-deficient medium + 1-mM Mg^{2+} medium (four applications, right). (B) Superimposed records showing a slowing of receptor deactivation caused by repetitive agonist application (black) and by removal of Ca^{2+} (gray). (C) Comparison of the rates of current deactivation during prolonged (40 s) agonist application in the presence and absence of bath Ca^{2+}. 1 and 2 are the first and second agonist applications. (D) Dependence of the rates of receptor deactivation on Ca^{2+} concentrations. Representative traces (gray) and fitted biexponential curves (black). (inset) Bars indicate mean ± SEM values of τ_{off2}, and asterisks indicate significant difference ($P < 0.01$) versus 0 mM Ca^{2+}. $n = 5–10$ per data point. (E and F) Example records of change in the rates of current deactivation by replacing 2-mM Ca^{2+}–containing medium with Ca^{2+}-deficient medium (indicated by horizontal bars) in cells expressing the wild-type (E) and H130A mutant (F) P2X7Rs.

concentration-dependent manner (Fig. 3, H and I), which is highly comparable with that observed in cells clamped at −60 mV (Fig. 3, E and F). As Ca^{2+} influx would be negligible in this condition, the results suggest that Ca^{2+} probably does not act near the channel pore.

Calcium dependence of receptor deactivation

If bath Ca^{2+} allosterically affects the potency of orthosteric ligands at P2X7R, it should also affect the rates of receptor deactivation. In general, the washout of ATP was accompanied by a relatively rapid decline of current (deactivation), whereas the decline of the current after washout of the more potent BzATP was slower (Fig. 1). In concentrations that caused biphasic responses when cells were bathed in Ca^{2+}-containing medium, the best approximation for decay of current after the washout of agonist was achieved using biexponential fitting, and the averaged decay constants τ_1 and τ_2 were about sevenfold larger for BzATP than for ATP ($\tau_1 = 2.8 \pm 0.5$ vs. 0.4 ± 0.2 s; $\tau_2 = 14.9 \pm 1.1$ vs. 2.1 ± 0.2 s, respectively).

To study the effects of bath Ca^{2+} on the kinetics of receptor deactivation, we used several experimental approaches. In the first experiment, the same cells were repetitively stimulated with 100 μM BzATP for 1 s separated by washout periods of 2 min in 2-mM Ca^{2+}–containing medium (Fig. 4 A, left) or 4 min in Ca^{2+}-deficient medium (Fig. 4 A, right). Superimposed records from these experiments show two phenomena. First, deactivation of receptors was dramatically slowed in cells bathed in Ca^{2+}-deficient medium, indicating that bath Ca^{2+} reduces the potency of agonist. Second, repetitive stimulation slowed receptor deactivation independently of the status of bath Ca^{2+} (Fig. 4 B). Both phenomena were also observed during repetitive application of 100 μM BzATP for 40 s (Fig. 4 C).

The effect of bath Ca^{2+} on receptor deactivation was concentration dependent. Fig. 4 D (left) shows representative traces (gray) with fitted biexponential curves (black) from cells bathed in media containing 0.5, 5, and 10 mM Ca^{2+}. From the fitting curves, the τ_2s were derived, and the mean ± SEM values were generated (Fig. 4 D, inset). To study the time course of Ca^{2+} action, we replaced 2 mM Ca^{2+}–containing medium with Ca^{2+}-deficient medium (Fig. 4 E, horizontal bars) during washout of agonists. The addition of Ca^{2+} rapidly (0.5 s) and reversibly affected the rate of receptor deactivation. The same effect was also observed in cells expressing P2X7R-H130A mutant (Fig. 4 F). Thus, bath Ca^{2+} rapidly, and in a concentration-dependent manner, facilitates receptor deactivation.

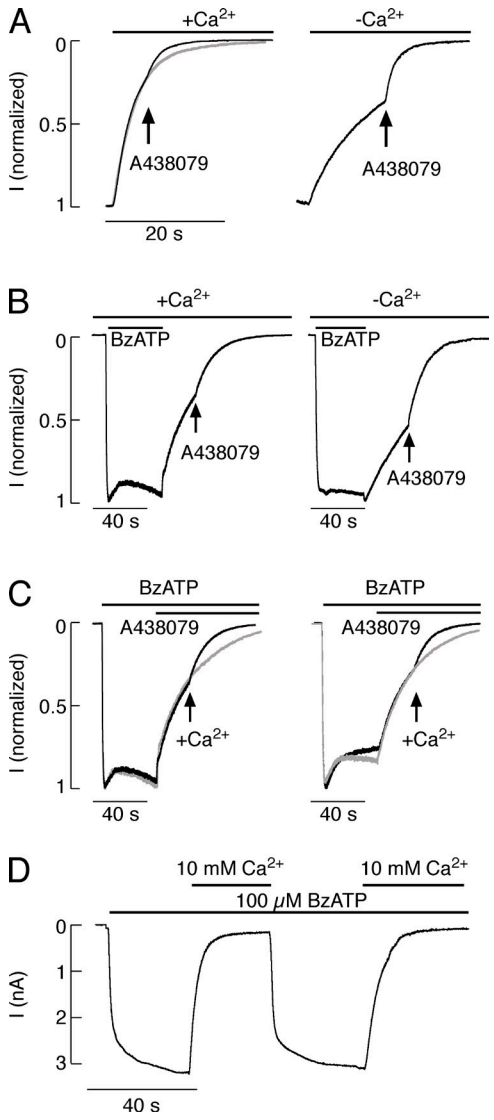

Figure 5. Comparison of the effects of bath Ca^{2+}, A438079, and CBX on the rates of receptor deactivation. (A) Effects of A438079 application on the rate of deactivation of the wild-type P2X7R after washout of 100 µM BzATP with 2-mM Ca^{2+}–containing (left) and Ca^{2+}-deficient (right) medium. The gray trace (left) shows receptor deactivation in the absence of A438079. For clarity, the activation phase is not shown. (B) Changes in the rate of T15E-P2X7R deactivation by application of 100 µM A438079 in cells bathed in 2-mM Ca^{2+}–containing (left) and Ca^{2+}-deficient (right) medium. (C) Two examples of effects of 2 mM Ca^{2+} on the rate of T15E-P2X7R deactivation in the presence of A438079. Arrows indicate the time of Ca^{2+} application; black traces, 2 mM Ca^{2+}; gray traces, Ca^{2+}-deficient medium. In all experiments, bath medium contained 1 mM Mg^{2+}, cells were stimulated with 100 µM BzATP, and the concentration of A438079 was 100 µM. (D) Effects of 10 mM Ca^{2+} on the amplitude of 100-µM BzATP–induced current in cells expressing the wild-type receptor and bathed in Ca^{2+}-deficient medium with 32 µM CBX.

Effects of A438079 and carbenoxolone (CBX) on receptor activation and deactivation

Facilitation of receptor deactivation by bath Ca^{2+} could be explained either by inhibition of the rebound effect of BzATP on current or by facilitated dissociation of residual bound agonist from binding sites, the latter being consistent with allosteric action of this cation. To clarify this issue, in further studies we used A438079 (Torcis), a human P2X7R-specific competitive antagonist (Nelson et al., 2006; McGaraughty et al., 2007). In cells expressing rat P2X7R, A438079 applied alone did not generate any current (unpublished data). When applied together with 3.2 mM ATP, it reduced the peak amplitude of current in a concentration-dependent manner (Fig. S1 A), with an estimated IC_{50} value of ~1 µM. A438079 also concentration dependently inhibited 100-µM BzATP–induced current amplitude (Fig. S1 B) with a similar IC_{50} value. Furthermore, in cells with developed biphasic current caused by the application of 100 µM BzATP, A438079 rapidly and in a dose-dependent manner decreased the peak amplitude of current with an IC_{50} value of ~0.3 µM (Fig. S1 C). When cells were stimulated with 32 µM BzATP, A438079 also inhibited current with an IC_{50} of ~0.3 µM. Together, these data show that A438079 also acts as a typical competitive orthosteric antagonist to rat receptor, with ~3,000-fold higher potency than ATP and 200-fold higher potency than BzATP, and could be used to study effects of calcium on the kinetics of receptor deactivation.

Fig. 5 A shows that A438079 facilitated deactivation of the wild-type receptor in both Ca^{2+}-containing (left) and Ca^{2+}-deficient medium (right) and that this effect was rapid (~0.8 s). To further clarify this issue, we used the T15E-P2X7R mutant, which is more sensitive to BzATP and, consequently, deactivates slowly (Yan et al., 2010). When applied during the washout of free BzATP, A438079 also facilitated the mutant receptor deactivation. The effect of A438079 of increasing the rate of receptor deactivation was observed in cells bathed in both Ca^{2+}-containing and -deficient medium (Fig. 5 B). These results indicate that BzATP is partially rebound during the washout period and is replaced by a more potent ligand molecule. When deactivation of receptors was initiated by washing the cells with Ca^{2+}-deficient medium in the presence of A438079, the subsequent addition of 2 mM Ca^{2+} facilitated receptor deactivation (Fig. 5 C). These results indicate that the rapid effect of bath Ca^{2+} on the current decay during the washout period is not dependent on the rebinding effect of orthosteric agonists on P2X7R gating.

In our experimental conditions, HEK293 cells express mRNA transcripts for pannexin-1 (Panx1), but not Panx2 and Panx3. The expression of Panx1 protein transcripts was below detection by Western blot analysis (Li et al., 2011). The inhibitory effect of Ca^{2+} on receptor activation was preserved in cells treated with 32 µM CBX, an inhibitor of Panx1 channels. Fig. 5 D shows the inhibitory effect of 10 mM Ca^{2+} on 100-µM BzATP–induced current in cells expressing the wild-type receptor and perfused with Ca^{2+}-deficient medium containing 32 µM

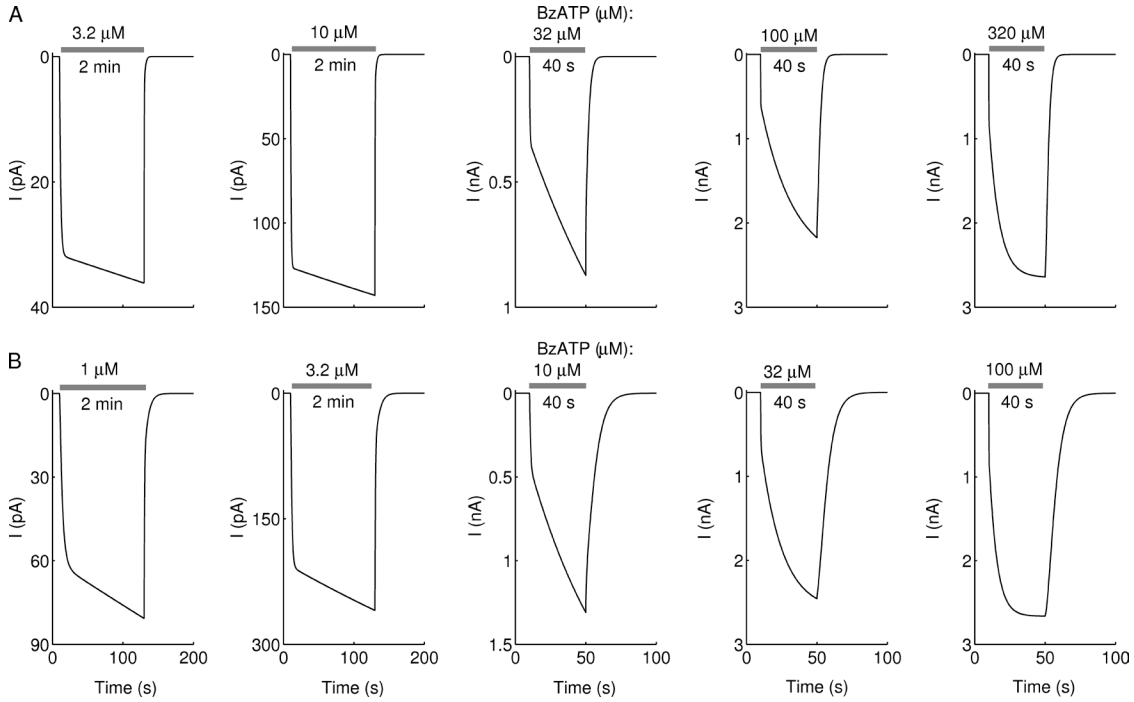

Figure 6. Dependence of current simulations on BzATP and extracellular calcium concentrations. (A and B) Current simulations generated by the kinetic model, Eqs. 1–9, in the presence of 2 mM Ca^{2+} (A) and in the absence (B) of bath Ca^{2+} during 40-s and 2-min BzATP stimulation at increasing doses, as specified by the gray bars. Monophasic and biphasic responses are obtained at low and high concentrations of BzATP, respectively, in both cases, a result consistent with the experimental recordings (Fig. 1). The loss of allosteric inhibition exerted by extracellular Ca^{2+} in B led to an increase in the potency of BzATP, which manifested itself in requiring less agonist concentration (a reduction of ∼70% compared with A) to produce the same response.

CBX. These data indicate that even if Panx1 channels are expressed in HEK293 cells in sufficient numbers, their interaction with P2X7R does not account for inhibition of receptor function by Ca^{2+}. Together with the findings that bath Ca^{2+} affects receptor activation in a concentration-dependent manner and independently of free agonist concentration, these experiments definitively show that Ca^{2+} in physiological concentrations acts as a negative allosteric modulator.

Kinetic model for calcium-dependent allosteric regulation

To have a better understanding of the effects of bath Ca^{2+} on P2X7R channel gating, we used a Markov state model consistent with the model presented in Yan et al. (2010), except for the inclusion of the allosteric regulation exerted by $[Ca^{2+}]_e$ on the P2X7Rs, which was suggested by the experimental results presented in Figs. 1–4. This was done by assuming that $[Ca^{2+}]_e$ increases the backward rates (k_1, k_3, and k_5) by the fraction $2 - F$ and decreases the forward rates (k_2, k_4, and k_6) by the fraction F. In Fig. 6, we show current simulations (obtained using Eq. 9) generated by stimulating model cells (described by Eqs. 1–8) with increasing doses of agonist (BzATP) concentrations at two different levels of $[Ca^{2+}]_e$: 2 and 0 mM. At 2-mM $[Ca^{2+}]_e$, current simulations were similar to those shown in Fig. 1 C (and identical to the ones displayed in Yan et al. [2010] under the same conditions). To briefly summarize our results, we found that the model exhibited monophasic slow current responses at low BzATP concentrations (3.2 and 10 μM) and biphasic current responses that included fast and slow components at high BzATP concentrations (32, 100, and 320 μM) during both the activation and deactivation phases of the current. We suggested in Yan et al. (2010) that the slow component of the current exhibited at high agonist concentrations is a result of the sensitization of receptors (i.e., dilation of the channel pores associated with these receptors). This corresponds to a shift in the fraction of receptors in the top row to the bottom row of Fig. S2. The fast component of the activation phases gradually dominated over the slow component as the agonist concentration was increased. With the additional feature included in the model, subjecting the model cells to Ca^{2+}-deficient medium ($[Ca^{2+}]_e$ = 0 mM), as was done in Fig. 6 B, increased the potency of agonist binding (as a result of an increase in the value of the ratio $F/[2 - F]$). A reduction in agonist concentration by 0.5 log units generated the same outcomes obtained in Fig. 6 A, consistent with the cell recordings shown in Fig. 1 (C and D).

To investigate the effect of extracellular Ca^{2+} (or divalent cations in general) on current amplitudes, we stimulated a single model cell with 100 μM BzATP and only varied $[Ca^{2+}]_e$. Fig. 7 A shows that the simulated current

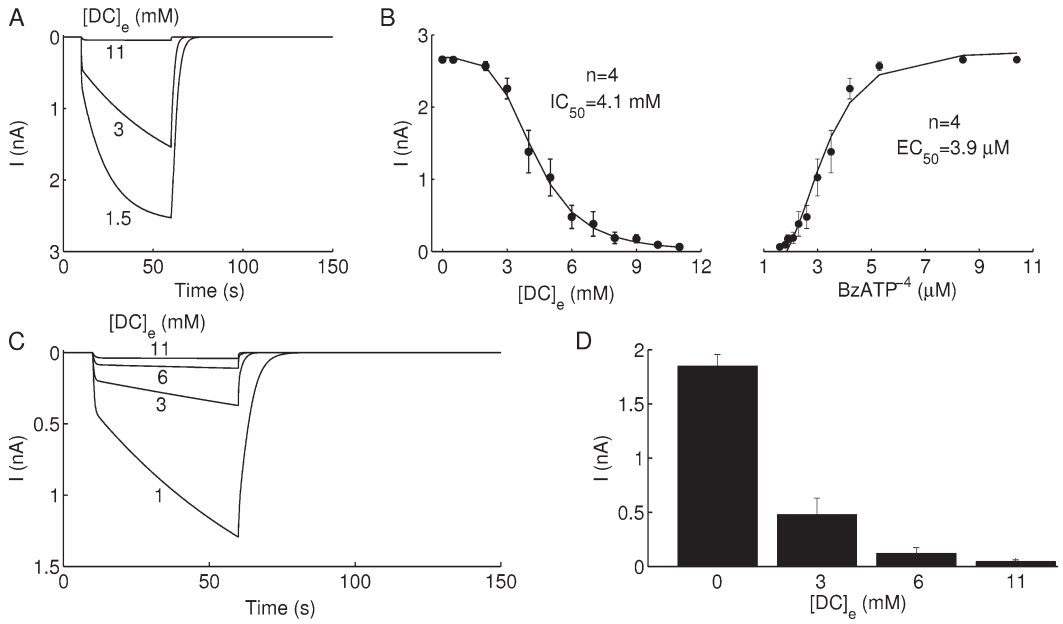

Figure 7. Dependency of current amplitudes on $[Ca^{2+}]_e$ and free BzATP agonist concentrations, as determined by the kinetic model, Eqs. 1–9. (A) Stimulating the kinetic model with 100 µM BzATP at three levels of $[Ca^{2+}]_e$, 0.5, 2, and 10 mM in the presence of 1 mM Mg^{2+}, shows a decrease in current amplitude during $[Ca^{2+}]_e$ increase. (B) Best fit to the $[Ca^{2+}]_e$-dependent (left) and free BzATP–dependent (right) dose–response curves of current amplitudes, obtained from stimulating a heterogeneous population of 10 model cells (each generated by randomly selecting parameter values from the distributions listed in Table S1) with 100 µM BzATP. The $[Ca^{2+}]_e$-dependent dose–response curve is a decreasing Hill function, whereas the free BzATP–dependent dose–response curve is an increasing Hill function. (C) As in Fig. 3 E, current amplitudes obtained from stimulating the kinetic model with identical free BzATP concentrations, achieved by variable BzATP and $[Ca^{2+}]_e$, decrease with $[Ca^{2+}]_e$ increase. (D) As in Fig. 3 F, current amplitudes obtained from a heterogeneous population of 10 model cells exhibit a decrease with $[Ca^{2+}]_e$ during stimulation with identical concentrations of free BzATP in each simulation. Error bars indicate mean ± SEM values of current amplitude.

amplitudes decreased in proportions similar to those observed experimentally when $[Ca^{2+}]_e$ was gradually increased from 1.5 to 3 and then to 11 mM (compare with Fig. 3 B). Extending this result to a heterogeneous population of model cells (randomly generated from the distributions listed in Table S1) stimulated by the same level of BzATP concentration (100 µM) and subjected to various levels of $[Ca^{2+}]_e$ (between 0.5 and 10 mM) with fixed (1 mM) Mg^{2+} concentration revealed that the Ca^{2+}-dependent dose–response curve for the current amplitude generated by the whole population, shown in Fig. 7 (B, left), is best fitted by a decreasing Hill function, with a Hill coefficient of $n = 4$ and half-maximum inhibition of $IC_{50} = 4.1$ mM. The best fit to the $BzATP^{4-}$-dependent dose–response curve, shown in Fig. 7 (B, right), was an increasing Hill function with $n = 4$ and $EC_{50} = 3.9$ µM (where $BzATP^{4-}$ at each data point was calculated in a manner similar to that described in the Materials and methods section). It should be mentioned here that even if the effect of extracellular Ca^{2+} was modeled differently, e.g., by assuming that F is a linearly decreasing function of $[Ca^{2+}]_e$ (considered experimentally unrealistic), we would still get a Hill-like function for both Ca^{2+}- and free BzATP–dependent dose–response curves (unpublished data). It is possible that the fit in Fig. 3 C is linear because of the small number of data points; with data at a greater number of concentrations, the experimental curve might turn out to be sigmoidal, as suggested here.

The P2X7R inhibition observed in Fig. 7 (A and B) is clearly not caused by a decrease in free agonist concentration (as a result of Ca^{2+} binding) because F and $2 - F$ do not reflect this feature but rather the allosteric regulation. To confirm this, we repeated the same experimental procedure conducted in Fig. 3 (D–F) by initially stimulating a single model cell with the same level of free BzATP (obtained by varying both extracellular Ca^{2+} and BzATP concentrations in a manner similar to Fig. 3 D). Fig. 7 C shows that the simulated current amplitudes decreased with the increase in $[Ca^{2+}]_e$, which is compatible with an allosteric regulation of the receptor by Ca^{2+}. Extending this idea to a heterogeneous population of model cells, as in Fig. 7 D, revealed that a negative correlation exists between current amplitudes and $[Ca^{2+}]_e$, even though free BzATP in each case is the same, an outcome consistent with the experimental results in Fig. 3 E.

The main advantage of using kinetic models of this nature is the ability to extract quantitative information about the fraction of receptors in each state. This may provide insight into how extracellular Ca^{2+} allosterically inhibits receptor activation and facilitates receptor deactivation. For this reason, we have simulated in Fig. 8 the time evolution of the two closed states, C_1 (black) and C_4 (gray)

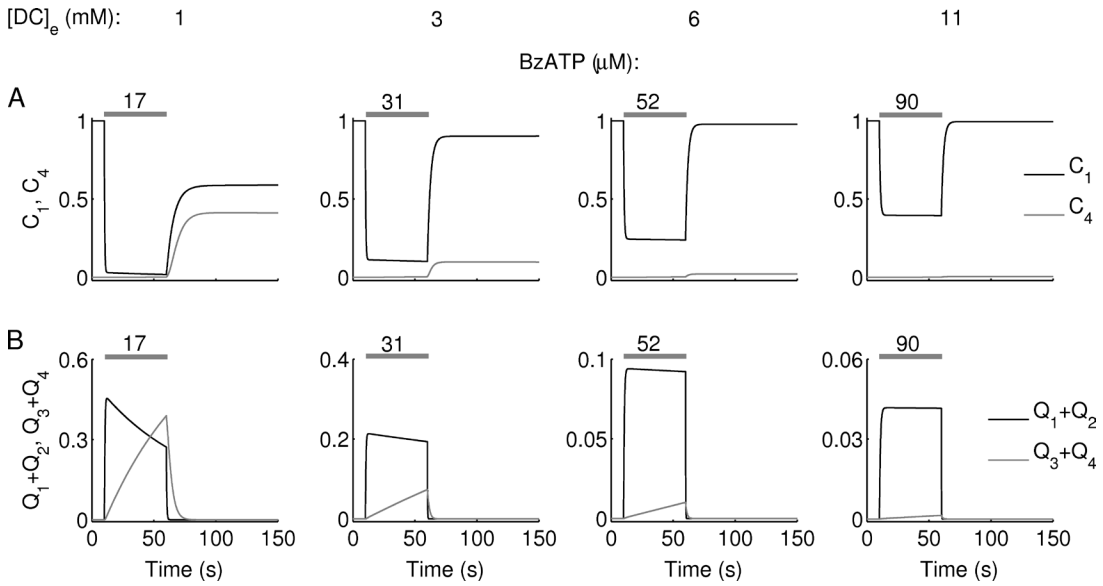

Figure 8. Simulated response to a 1-min stimulation with various concentrations of BzATP. Gray bars indicate the various concentrations of BzATP. (A) Fraction of receptors in the two closed states, C_1 (black) and C_4 (gray). (B) Fraction of receptors in open states, $Q_1 + Q_2$ (black), and dilated states, $Q_3 + Q_4$ (gray). Free BzATP in each stimulation was identical. As in Fig. 7 C, this was achieved by variable BzATP and $[Ca^{2+}]_e$ (identified by the $[DC]_e$ values, top row). Increased $[Ca^{2+}]_e$ increases the allosteric inhibition of P2X7R and thus reduces receptor sensitization and pore dilation (i.e., leads to a shift to the bottom row of Fig. S2).

in A, and the two open states, $Q_1 + Q_2$ (black) and $Q_3 + Q_4$ (gray) in B, to illustrate how maintaining the same level of free BzATP (by varying $[Ca^{2+}]_e$ and BzATP concentration identified by the $[DC]_e$ values and gray bars in Fig. 8, respectively) could produce the effects observed in Figs. 3 and 7. Fig. 8 A shows that even though the increase in $[Ca^{2+}]_e$ only decreased the activation of naive states slightly, the accumulation of receptors in $Q_1 + Q_2$ was significantly reduced (Fig. 8 B), leading to a significant reduction in the sensitization of receptors quantified by the fraction $Q_3 + Q_4$ (during stimulation) and C_4 (during washout). This explains the progressive loss of the slow component (I_2) of the activation phase of the current observed in Figs. 3 E and 7 C. The loss of the sensitized receptor component is also responsible for the loss of the slow deactivation component at high agonist concentration (Fig. S4). This explains the increase in the deactivation rate observed in Fig. 7 C.

The dependency of the deactivation phase of current on extracellular Ca^{2+} observed in Fig. 3 was also reproduced by the model, as shown in Fig. 9. Activation of a naive model cell repeatedly with 100 μM BzATP for 1 s (Fig. 9 A) in the presence of 2 mM Ca^{2+} (Fig. 9 A, left) and the absence of extracellular Ca^{2+} (Fig. 9 A, right) showed that it takes longer for the current to go back to baseline in the latter case (55 s) than in the former (11 s). This is confirmed in Fig. 9 B, where the simulated currents obtained in each BzATP pulse, normalized by their maximum values, exhibited a faster deactivation phase in Ca^{2+}-containing medium (black) than in Ca^{2+}-deficient medium (gray). Furthermore, subsequent pulses showed slower deactivation than the former pulses in both the presence and absence of external Ca^{2+} as a result of receptor sensitization, as was previously described in Yan et al. (2010). As illustrated in Fig. 8, the allosteric inhibition exerted by Ca^{2+} led to a reduction in receptor accumulation in state Q_2, causing a decrease in the fraction of sensitized receptors (i.e., a decline in the number of P2X7Rs transitioning from the top row to the bottom row of Fig. S2). Consequently, during washout, the deactivation phase at higher $[Ca^{2+}]_e$ is primarily governed by the backward rates (k_1, k_3, and k_5) of the unsensitized states (Fig. S2, top row), which are faster than those (k_1) of the sensitized states (Fig. S2, bottom row), in contrast to the behavior in Ca^{2+}-deficient medium (see Fig. S4 for the breakdown into sensitized and unsensitized receptors). Increasing the duration of stimulation to 40 s in Fig. 9 C resulted in similar outcomes; namely, slower deactivation phases in the absence of extracellular Ca^{2+} for both first (left) and second pulses (right). In other words, such behavior was independent of how long the model cells were stimulated for.

To further examine the effects of various concentrations of extracellular Ca^{2+} on the deactivation phase of the current, we subjected a naive model cell, stimulated with 100 μM BzATP for 40 s, to 0.5-, 5-, and 10-mM $[Ca^{2+}]_e$. The deactivation phases of simulated currents, normalized by their maximum values and shown in Fig. 9 (D, left), exhibited similar outcomes to those observed experimentally in Fig. 4 D: the increase in $[Ca^{2+}]_e$ led to a progressive increase in the rate of receptor deactivation. Extending this study to a heterogeneous population of 10 model cells subjected to 0-, 0.5-, 2-, and 5-mM $[Ca^{2+}]_e$ and stimulated with 100 μM BzATP revealed that the average time

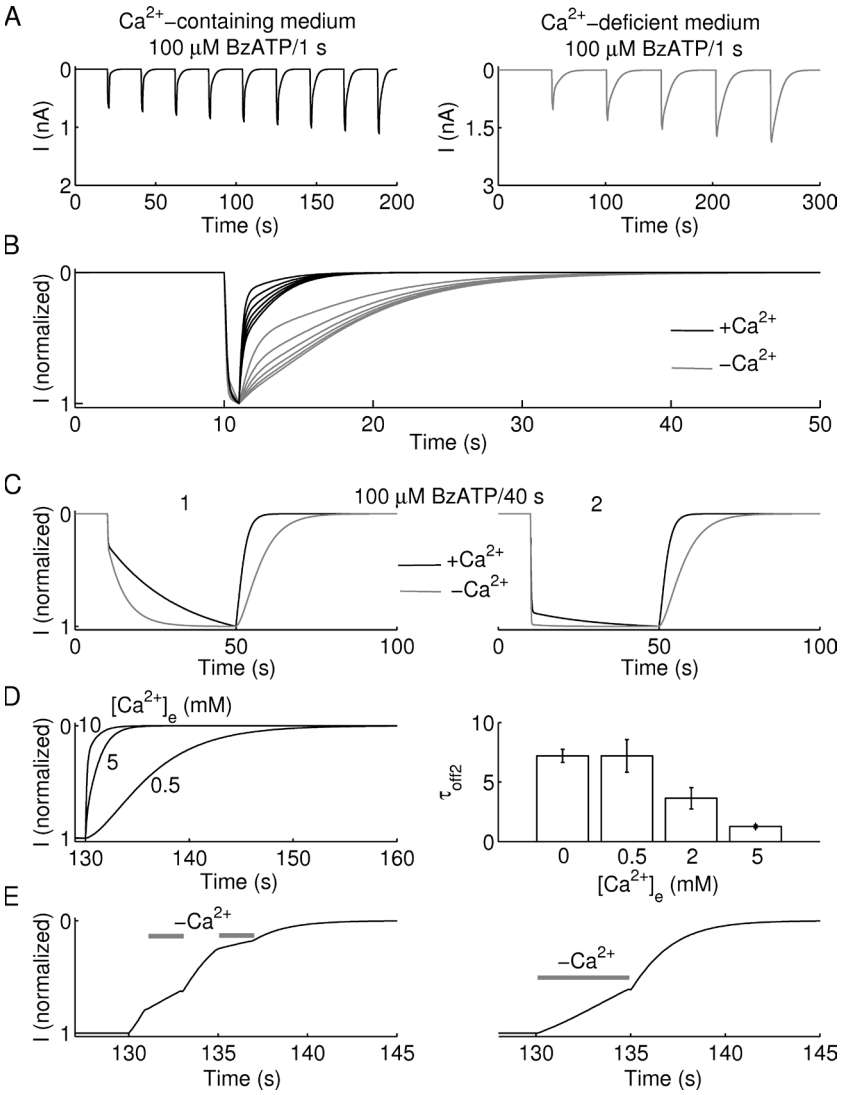

Figure 9. Dependence of P2X7R deactivation on $[Ca^{2+}]_e$ as determined by the kinetic model, Eqs. 1–9. (A) Repetitive 1-s stimulation with 100 µM BzATP in the presence of 2 mM (left) and in the absence (right) of extracellular Ca^{2+} (compare with Fig. 4 A). (B) Currents from A normalized by their maximum amplitudes show that the deactivation components of these currents are slower in Ca^{2+}-deficient medium (gray) than in Ca^{2+}-containing medium (black). Slowing of deactivation with each subsequent pulse occurs with or without extracellular Ca^{2+} (compare with Fig. 4 B). (C) Stimulating the kinetic model with 100 µM BzATP for 40 s in the presence (black) and absence (gray) of extracellular Ca^{2+} and normalizing current amplitudes by their maximum values result in both faster sensitization (and pore dilation) and also slower deactivation in the absence of extracellular Ca^{2+} during both the first (left) and second (right) stimulations (compare with Fig. 4 C). (D) Deactivation components normalized by their maximum values during 100-µM BzATP stimulation for 40 s. Decreasing $[Ca^{2+}]_e$ from 10 to 5 and then 0.5 mM slows deactivation (left). The slow time constant τ_{off2} (right), obtained from fitting biexponential curves to the deactivation curves obtained from stimulating 10 heterogeneous populations of simulated cells, decreases with $[Ca^{2+}]_e$ (compare with Fig. 4 D). Error bars indicate mean ± SEM values of τ_{off2}. (E) Calcium removal during P2X7R deactivation at two disjointed 2-s intervals (left) and one 5-s interval (right) results in slower deactivation (compare with Fig. 4, E and F). Simulated currents were generated for a 40-s application of 100 µM BzATP in the presence of 2-mM $[Ca^{2+}]_e$ and normalized by their maximum values.

constant τ_{off2}, obtained from fitting a biexponential function to the deactivation phases, decreased as $[Ca^{2+}]_e$ was increased, a result consistent with the experimentally observed outcomes in Fig. 4 D. As indicated earlier, the decrease is caused by a gradual loss of the sensitized compartment responsible for the slow deactivation (as illustrated in Fig. 8 and Fig. S4). Finally, alternating $[Ca^{2+}]_e$ between 2 and 0 mM during the deactivation phase of the simulated current only (as shown in Fig. 9 E) repetitively for 3 s (left) or once for 5 s at the onset of the deactivation phase (right) exhibited similar outcomes to those observed in Fig. 4 E; namely, fast deactivation at high $[Ca^{2+}]_e$, slow deactivation at low $[Ca^{2+}]_e$, and instantaneous change between these two distinct behaviors once the $[Ca^{2+}]_e$ is altered.

DISCUSSION

We have shown here that the agonistic actions of ATP and BzATP on P2X7R were affected by bath Ca^{2+} concentration in the presence of fixed Mg^{2+} concentration (1 mM). Consistent with findings by others (Surprenant et al., 1996; Virginio et al., 1997; Klapperstück et al., 2001), bath Ca^{2+} inhibited agonist-induced current in a concentration-dependent manner, causing a rightward shift in dose–response experiments. In our experimental conditions with naive receptors, the difference was ~0.5 log units when cells were bathed in Ca^{2+}-deficient and 2-mM Ca^{2+}–containing medium. For P2X4R, it has also been shown that bath Ca^{2+} affects the permeability state of the receptor; in the presence of bath Ca^{2+}, the channel is only permeable to small cations, whereas in cells bathed in Ca^{2+}-deficient medium, the channel pore is permeable to larger organic cations (Khakh et al., 1999). This finding was confirmed more recently using fast-scanning atomic force microscopy (Shinozaki et al., 2009).

Initially, it was suggested that P2X7R is activated rapidly (within milliseconds) after application of agonists, followed by a gradual (within seconds to minutes) increase in permeability to organic cations and fluorescent dyes (Surprenant, 1996; Chessell et al., 1997;

Michel et al., 1999), which parallels the presence of I_1 and I_2 in our experiments. However, several observations suggest that fluorescent dye entry occurs through a separate pathway than organic cations (Petrou et al., 1997; Klapperstück et al., 2000), and the coupling of P2X7R to Panx1 channels was suggested to account for cellular entry of fluorescent dyes (Pelegrin and Surprenant, 2006). Our recent data on this topic are consistent with the original hypothesis of P2X7R pore dilating during the sustained agonist application, including the finding that I_2 current growth temporally coincides with the transition from an open to a dilated state (Yan et al., 2008, 2010). Here, we show that removal of bath Ca^{2+} was not essential for the development of a secondary current growth (Fig. 1). Dilation of the P2X2R pore also does not require removal of bath Ca^{2+} (Chaumont and Khakh, 2008). Our data do not exclude the possibility that Panx1 contributes to dye uptake in P2X7R-expressing HEK293 cells and do not argue against the role of Panxs in other purinergic signaling functions. Several recent publications (Dubyak, 2009), including our own work (Li et al., 2011), indicate that Panxs release ATP and that this action may include interactions with P2XRs.

A rightward shift in the potency of two orthosteric agonists in cells bathed in medium containing 2 mM Ca^{2+} was not visible when the calculated free agonist concentration was used in concentration response relationship analysis. Others have reached similar conclusions in experiments using Ca^{2+}-deficient medium and manipulating bath Mg^{2+} concentrations (Klapperstück et al., 2001; Liu, M., S.D. Silberberg, and K.J. Swartz. 2011. ATP^{4-} activates P2X receptors. Annual Biophysical Meeting. 1472-Pos.). This is consistent with the hypothesis that ATP^{4-}, rather than the divalent-bound ATP, is the native agonist for this receptor subtype (Dahlquist and Diamant, 1974; Cockcroft and Gomperts, 1979; Di Virgilio et al., 1998).

However, these experiments do not exclude the possibility that 2 mM Ca^{2+} causes a rightward shift in the potency of agonists of ~0.5 log units independently of the concentration of the free acid form of agonists. To overcome limitations in the interpretation of such data, we performed experiments with variable agonist and bath Ca^{2+} concentrations leading to a constant free agonist concentration. Under such experimental conditions, we still observed a concentration-dependent inhibitory effect of bath Ca^{2+} on receptor functions, clearly indicating that this cation exerts inhibitory effects on gating independently of the concentration of orthosteric agonists. Recently, it was shown that the rP2X7R-H130A mutant is resistant to Mg^{2+} inhibition (Acuña-Castillo et al., 2007), reinforcing the hypothesis that this metal also acts through an allosteric mechanism. Here, we showed that this residue does not account for the effects of Ca^{2+} on agonist-induced activation of receptors. We also showed that Ca^{2+} does not act near the channel pore. Finally, our data argue against the hypothesis that Ca^{2+} effects on P2X7R activation is through Panx1 interacting with P2X7R. First, the expression of Panx1 protein in HEK293 cells in our experiments is very low, below the detection by Western blot analysis (Li et al., 2011), and P2X7R protein is overexpressed, suggesting that only a small fraction of receptors could be associated with Panx1, in contrast to almost complete inhibition of current by 10 mM Ca^{2+}. Second, in cells bathed in medium containing 32 µM CBX, an inhibitor of Panx1 channels, the inhibitory effect of high Ca^{2+} on P2X7R activation was not changed.

In our study, the application of agonists and antagonist and their removal was performed using an ultrarapid perfusion system with good time resolution (Yan et al., 2006). In general, the time required for washout of agonist inversely correlates with the potency of agonist for binding sites (Rettinger and Schmalzing, 2004). Consistent with this conclusion, we observed that the reduced potency of ATP compared with BzATP to activate P2X7R was accompanied by a rapid decay of current after washout of ATP and a slow decay of current after washout of BzATP. We also observed that removal of Ca^{2+} in the presence of 1 mM Mg^{2+} slowed the rates of receptor deactivation in a concentration- and time-dependent manner, further supporting the conclusion that bath Ca^{2+} affects the potency of agonist. However, during repetitive agonist application, we observed a progressive decrease in the rates of receptor deactivation, which we previously termed receptor sensitization (Yan et al., 2010). Here, we showed that this process occurs in both Ca^{2+}-containing and -deficient medium, indicating that, like pore dilation, sensitization of receptors is not influenced by bath Ca^{2+}.

To study the influence of allosteric ligands on the occupancy of P2X7R orthosteric sites, others have analyzed receptor deactivation in the presence and absence of orthosteric and allosteric agonists and antagonists (Bianchi and Macdonald, 2001). Previous studies indicated that A438079 is a human P2X7R-specific competitive antagonist (Nelson et al., 2006; McGaraughty et al., 2007). Our experiments showed that this compound also acts as a competitive orthosteric antagonist for rP2X7R. The potency of this antagonist was 200-fold higher than BzATP, a critical feature in experiments on the kinetics of receptor deactivation.

When A438079 was applied during the washout period, it facilitated deactivation in Ca^{2+}-containing and Ca^{2+}-deficient medium with similar rates. The same results were obtained with the T15E-P2X7R mutant, which is more sensitive to BzATP and, consequently, deactivates more slowly (Yan et al., 2010). We interpreted this observation as an indication that a fraction of BzATP released from the binding domain during the washout period rebinds, and that process is reduced or abolished in the presence of a more potent competitive antagonist. We also observed that deactivation of receptors in the

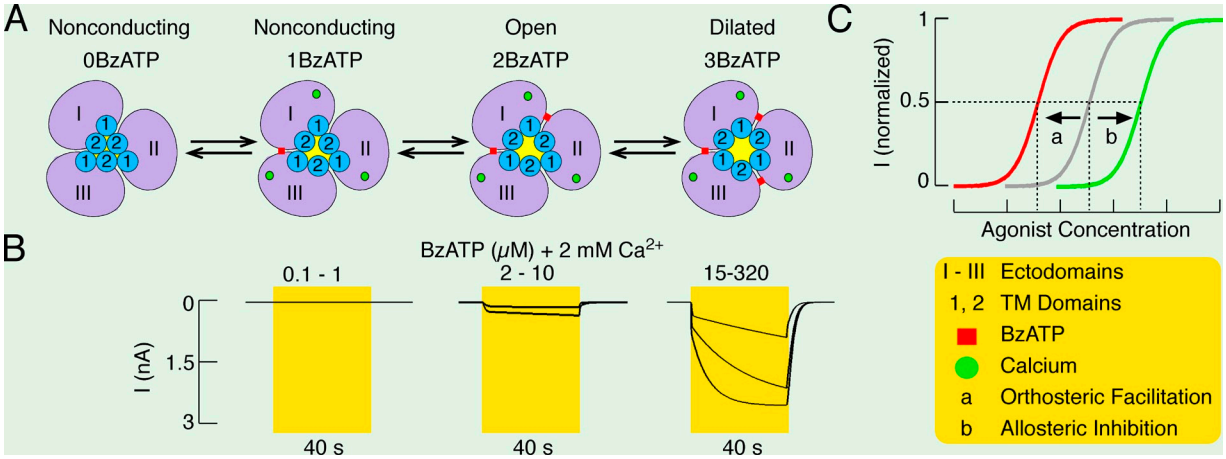

Figure 10. Orthosteric (BzATP) facilitation and allosteric (Ca^{2+}) inhibition of P2X7R. (A) In resting conditions (no agonist bound), the naive P2X7R is a symmetrical trimer, with three binding sites having equal and high affinity for orthosteric agonists, and is closed. The occupation of one binding site by agonist does not open the pore but leads to the loss of symmetry and an assumed reduction in the affinity of the two remaining binding sites as a result of a conformational change. When a second site is occupied, the affinity of the remaining binding site is further reduced, but the channel opens in a low conductance state. When three binding sites are occupied, however, symmetry is restored, and the binding rates revert to those of a naked receptor, allowing the pore to gradually dilate to a high conductance state and to sensitize. (B) The naive receptor in the open state generates monophasic currents with peak amplitude determined by BzATP concentration. The naive receptor at high BzATP concentration dilates and generates high amplitude biphasic currents. (C) Dependence of the peak current amplitude, measured 40 s after agonist application, on orthosteric and allosteric agonist concentrations. Gray trace, concentration dependence on BzATP of the peak current response of naive receptors in the presence of physiological bath Ca^{2+} concentration. Red trace, concentration dependence on BzATP of the peak current response of sensitized receptors, termed orthosteric facilitation, in the presence of physiological Ca^{2+} concentration. Green trace, concentration dependence on BzATP of the peak current response of naive receptors in the presence of elevated bath Ca^{2+}. For details on orthosteric facilitation, see Yan et al. (2010). Experiments presented in this manuscript show that the rightward shift in the potency of agonist to activate P2X7R reflects allosteric inhibition of the receptor by this cation.

presence of A438079 is facilitated by the addition of Ca^{2+} to bath medium, clearly indicating that the effect of Ca^{2+} on the rate of receptor deactivation is also present under conditions in which the rebinding effect of BzATP on the rate of deactivation was practically eliminated.

Some of these features of P2X7Rs were better understood by using a minimal kinetic Markov state model that incorporated not only the orthosteric regulation exerted by the agonist (which could lead to receptor sensitization) but also the allosteric regulation exerted by extracellular Ca^{2+}. The model, which was previously developed in Yan et al. (2010), integrated the allostery of Ca^{2+} in a simplified manner by assuming that an increase in $[Ca^{2+}]_e$ accelerated agonist unbinding and impeded agonist binding by factors that depended sigmoidally on $[Ca^{2+}]_e$. This model not only preserved the essential properties of current recording associated with agonist stimulation but also captured the diverse effects of $[Ca^{2+}]_e$ on the channel. It showed that the loss of the second phase of the current at high $[Ca^{2+}]_e$ is caused by a decline in the number of sensitized receptors, which in turn led to an increase in the rate of deactivation, because backward rates of unsensitized receptors are faster than those of sensitized receptors. The model also revealed that Ca^{2+}-dependent and free BzATP–dependent dose–response curves obtained from a heterogeneous population of model cells are (decreasing and increasing, respectively) Hill-like functions with $n = 4$ and $IC_{50} = 4.1$ mM for the former and $EC_{50} = 3.9$ μM for the latter. The structures of these response curves were found to be independent of the assumed Ca^{2+} dependency of the inhibition, suggesting that the experimental dose–response curves obtained here might be affected by the small number of concentrations used.

The effect of extracellular Ca^{2+} on P2X7R could have been modeled by including additional states characterizing the allosteric binding of Ca^{2+} to the receptor. The lack of information about the number of these binding sites and the potential increase in complexity of the kinetic model associated with such an approach prompted us to model this effect using Ca^{2+}-dependent Hill functions that directly acted on the binding and unbinding of the orthosteric agonist. Even though the use of this latter approach cannot determine how many allosteric binding sites the receptor may possess, it shows that the diverse effects of extracellular Ca^{2+} can all be accounted for by a common effect on binding and unbinding rates of agonist.

In summary, our investigations show that the binding of the orthosteric agonists ATP and BzATP to P2X7R causes gating transitions from closed to open to dilated states (Fig. 10 A), resulting in the generation of monophasic currents in intermediated concentration range and biphasic currents at higher agonist concentration

(Fig. 10 B). We further show that calcium influx is not required for conformations associated with pore dilation that coincide with the transition from low to high affinity states for orthosteric ligands, causing a leftward shift in the potency of agonists (Fig. 10 C) accompanied by a delay in receptor deactivation (orthosteric facilitation). We show by two independent tests that calcium in physiological concentrations acts as a negative allosteric modulator (or allosteric inhibitor): (1) by activating receptors with fixed free agonist concentrations and variable bath calcium concentrations and (2) by studying receptor deactivation in the presence and absence of P2X7R-specific competitive antagonist. Furthermore, we used a kinetic model to uncover how calcium exerts its allosteric regulation of these receptors. Systematic scanning of ectodomain residues is needed to identify amino acids responsible for allosteric actions of calcium.

We are thankful for constructive discussions with Drs. M. Tomic and C. Coddou and for H130A mutant from Dr. J.P. Huidobro-Toro.

The authors were supported by the Intramural Research Program of the National Institutes of Health, National Institute of Child Health and Human Development (grants to Z. Yan and S.S. Stojilkovic), and National Institute of Diabetes and Digestive and Kidney Diseases (grants to A. Khadra and A. Sherman).

Author contributions: Z. Yan carried out the bulk of the experiments, and A. Khadra did the modeling.

Lawrence G. Palmer served as editor.

Submitted: 6 April 2011
Accepted: 22 August 2011

REFERENCES

Acuña-Castillo, C., C. Coddou, P. Bull, J. Brito, and J.P. Huidobro-Toro. 2007. Differential role of extracellular histidines in copper, zinc, magnesium and proton modulation of the P2X7 purinergic receptor. *J. Neurochem.* 101:17–26. http://dx.doi.org/10.1111/j.1471-4159.2006.04343.x.

Bianchi, M.T., and R.L. Macdonald. 2001. Agonist trapping by GABAA receptor channels. *J. Neurosci.* 21:9083–9091.

Browne, L.E., L.H. Jiang, and R.A. North. 2010. New structure enlivens interest in P2X receptors. *Trends Pharmacol. Sci.* 31:229–237. http://dx.doi.org/10.1016/j.tips.2010.02.004

Chaumont, S., and B.S. Khakh. 2008. Patch-clamp coordinated spectroscopy shows P2X2 receptor permeability dynamics require cytosolic domain rearrangements but not Panx-1 channels. *Proc. Natl. Acad. Sci. USA.* 105:12063–12068. http://dx.doi.org/10.1073/pnas.0803008105

Chessell, I.P., A.D. Michel, and P.P. Humphrey. 1997. Properties of the pore-forming P2X7 purinoceptor in mouse NTW8 microglial cells. *Br. J. Pharmacol.* 121:1429–1437. http://dx.doi.org/10.1038/sj.bjp.0701278

Cockcroft, S., and B.D. Gomperts. 1979. Activation and inhibition of calcium-dependent histamine secretion by ATP ions applied to rat mast cells. *J. Physiol.* 296:229–243.

Coddou, C., Z. Yan, T. Obsil, J.P. Huidobro-Toro, and S.S. Stojilkovic. 2011. Activation and regulation of purinergic P2X receptor channels. *Pharmacol. Rev.* 63:641–683. http://dx.doi.org/10.1124/pr.110.003129

Colquhoun, D. 1998. Binding, gating, affinity and efficacy: the interpretation of structure-activity relationships for agonists and of the effects of mutating receptors. *Br. J. Pharmacol.* 125:923–947. http://dx.doi.org/10.1038/sj.bjp.0702164

Dahlquist, R., and B. Diamant. 1974. Interaction of ATP and calcium on the rat mast cell: effect on histamine release. *Acta Pharmacol. Toxicol. (Copenh.).* 34:368–384. http://dx.doi.org/10.1111/j.1600-0773.1974.tb03533.x

Di Virgilio, F., P. Chiozzi, S. Falzoni, D. Ferrari, J.M. Sanz, V. Venketaraman, and O.R. Baricordi. 1998. Cytolytic P2X purinoceptors. *Cell Death Differ.* 5:191–199. http://dx.doi.org/10.1038/sj.cdd.4400341

Dubyak, G.R. 2009. Both sides now: multiple interactions of ATP with pannexin-1 hemichannels. Focus on "A permeant regulating its permeation pore: inhibition of pannexin 1 channels by ATP". *Am. J. Physiol. Cell Physiol.* 296:C235–C241. http://dx.doi.org/10.1152/ajpcell.00639.2008

Egan, T.M., D.S. Samways, and Z. Li. 2006. Biophysics of P2X receptors. *Pflugers Arch.* 452:501–512. http://dx.doi.org/10.1007/s00424-006-0078-1

He, M.L., H. Zemkova, T.A. Koshimizu, M. Tomić, and S.S. Stojilkovic. 2003. Intracellular calcium measurements as a method in studies on activity of purinergic P2X receptor channels. *Am. J. Physiol. Cell Physiol.* 285:C467–C479.

Jahngen, J.H., and E.F. Rossomando. 1983. Resolution of an ATP-metal chelate from metal-free ATP by reverse-phase high-performance liquid chromatography. *Anal. Biochem.* 130:406–415. http://dx.doi.org/10.1016/0003-2697(83)90608-5

Jiang, L.H. 2009. Inhibition of P2X(7) receptors by divalent cations: old action and new insight. *Eur. Biophys. J.* 38:339–346. http://dx.doi.org/10.1007/s00249-008-0315-y

Khakh, B.S., X.R. Bao, C. Labarca, and H.A. Lester. 1999. Neuronal P2X transmitter-gated cation channels change their ion selectivity in seconds. *Nat. Neurosci.* 2:322–330. http://dx.doi.org/10.1038/7233

Klapperstück, M., C. Büttner, T. Böhm, G. Schmalzing, and F. Markwardt. 2000. Characteristics of P2X7 receptors from human B lymphocytes expressed in *Xenopus* oocytes. *Biochim. Biophys. Acta.* 1467:444–456. http://dx.doi.org/10.1016/S0005-2736(00)00245-5

Klapperstück, M., C. Büttner, G. Schmalzing, and F. Markwardt. 2001. Functional evidence of distinct ATP activation sites at the human P2X(7) receptor. *J. Physiol.* 534:25–35. http://dx.doi.org/10.1111/j.1469-7793.2001.00025.x

Li, S., I. Bjelobaba, Z. Yan, M. Kucka, M. Tomic, and S.S. Stojilkovic. 2011. Expression and roles of pannexins in ATP release in the pituitary gland. *Endocrinology.* 152:2342–2352. http://dx.doi.org/10.1210/en.2010-1216

Marquez-Klaka, B., J. Rettinger, Y. Bhargava, T. Eisele, and A. Nicke. 2007. Identification of an intersubunit cross-link between substituted cysteine residues located in the putative ATP binding site of the P2X1 receptor. *J. Neurosci.* 27:1456–1466. http://dx.doi.org/10.1523/JNEUROSCI.3105-06.2007

McGaraughty, S., K.L. Chu, M.T. Namovic, D.L. Donnelly-Roberts, R.R. Harris, X.F. Zhang, C.C. Shieh, C.T. Wismer, C.Z. Zhu, D.M. Gauvin, et al. 2007. P2X7-related modulation of pathological nociception in rats. *Neuroscience.* 146:1817–1828. http://dx.doi.org/10.1016/j.neuroscience.2007.03.035

Michel, A.D., I.P. Chessell, and P.P. Humphrey. 1999. Ionic effects on human recombinant P2X7 receptor function. *Naunyn Schmiedebergs Arch. Pharmacol.* 359:102–109. http://dx.doi.org/10.1007/PL00005328

Nelson, D.W., R.J. Gregg, M.E. Kort, A. Perez-Medrano, E.A. Voight, Y. Wang, G. Grayson, M.T. Namovic, D.L. Donnelly-Roberts, W. Niforatos, et al. 2006. Structure-activity relationship

studies on a series of novel, substituted 1-benzyl-5-phenyltetrazole P2X7 antagonists. *J. Med. Chem.* 49:3659–3666. http://dx.doi.org/10.1021/jm051202e

Nicke, A. 2008. Homotrimeric complexes are the dominant assembly state of native P2X7 subunits. *Biochem. Biophys. Res. Commun.* 377:803–808. http://dx.doi.org/10.1016/j.bbrc.2008.10.042

North, R.A. 2002. Molecular physiology of P2X receptors. *Physiol. Rev.* 82:1013–1067.

Pelegrin, P., and A. Surprenant. 2006. Pannexin-1 mediates large pore formation and interleukin-1beta release by the ATP-gated P2X7 receptor. *EMBO J.* 25:5071–5082. http://dx.doi.org/10.1038/sj.emboj.7601378

Petrou, S., M. Ugur, R.M. Drummond, J.J. Singer, and J.V. Walsh Jr. 1997. P2X7 purinoceptor expression in *Xenopus* oocytes is not sufficient to produce a pore-forming P2Z-like phenotype. *FEBS Lett.* 411:339–345. http://dx.doi.org/10.1016/S0014-5793(97)00700-X

Rettinger, J., and G. Schmalzing. 2004. Desensitization masks nanomolar potency of ATP for the P2X1 receptor. *J. Biol. Chem.* 279:6426–6433. http://dx.doi.org/10.1074/jbc.M306987200

Roger, S., P. Pelegrin, and A. Surprenant. 2008. Facilitation of P2X7 receptor currents and membrane blebbing via constitutive and dynamic calmodulin binding. *J. Neurosci.* 28:6393–6401. http://dx.doi.org/10.1523/JNEUROSCI.0696-08.2008

Shinozaki, Y., K. Sumitomo, M. Tsuda, S. Koizumi, K. Inoue, and K. Torimitsu. 2009. Direct observation of ATP-induced conformational changes in single P2X4 receptors. *PLoS Biol.* 7:e103. http://dx.doi.org/10.1371/journal.pbio.1000103

Surprenant, A. 1996. Functional properties of native and cloned P2X receptors. *Ciba Found. Symp.* 198:208–219.

Surprenant, A., F. Rassendren, E. Kawashima, R.A. North, and G. Buell. 1996. The cytolytic P2Z receptor for extracellular ATP identified as a P2X receptor (P2X7). *Science.* 272:735–738. http://dx.doi.org/10.1126/science.272.5262.735

Torres, G.E., T.M. Egan, and M.M. Voigt. 1999. Hetero-oligomeric assembly of P2X receptor subunits. Specificities exist with regard to possible partners. *J. Biol. Chem.* 274:6653–6659. http://dx.doi.org/10.1074/jbc.274.10.6653

Virginio, C., D. Church, R.A. North, and A. Surprenant. 1997. Effects of divalent cations, protons and calmidazolium at the rat P2X7 receptor. *Neuropharmacology.* 36:1285–1294. http://dx.doi.org/10.1016/S0028-3908(97)00141-X

Yan, Z., Z. Liang, M. Tomic, T. Obsil, and S.S. Stojilkovic. 2005. Molecular determinants of the agonist binding domain of a P2X receptor channel. *Mol. Pharmacol.* 67:1078–1088. http://dx.doi.org/10.1124/mol.104.010108

Yan, Z., Z. Liang, T. Obsil, and S.S. Stojilkovic. 2006. Participation of the Lys313-Ile333 sequence of the purinergic P2X4 receptor in agonist binding and transduction of signals to the channel gate. *J. Biol. Chem.* 281:32649–32659. http://dx.doi.org/10.1074/jbc.M512791200

Yan, Z., S. Li, Z. Liang, M. Tomic, and S.S. Stojilkovic. 2008. The P2X7 receptor channel pore dilates under physiological ion conditions. *J. Gen. Physiol.* 132:563–573. http://dx.doi.org/10.1085/jgp.200810059

Yan, Z., A. Khadra, S. Li, M. Tomic, A. Sherman, and S.S. Stojilkovic. 2010. Experimental characterization and mathematical modeling of P2X7 receptor channel gating. *J. Neurosci.* 30:14213–14224. http://dx.doi.org/10.1523/JNEUROSCI.2390-10.2010